Core-excited resonances in the dissociative recombination of CH^+ and CD^+

L. Carata* and A. E. Orel
Department of Applied Science, University of California Davis, Livermore 94550, California

M. Raoult
Laboratoire de Photophysique Moléculaire, Université de Paris–Sud, 91405 Orsay, France

I. F. Schneider* and A. Suzor-Weiner
Laboratoire de Photophysique Moléculaire, Université de Paris–Sud, 91405 Orsay, France
and Laboratoire de Chimie Physique, 11 rue Pierre et Marie Curie, 75234 Paris, France
(Received 15 December 1999; published 13 October 2000)

Storage-ring measurements of the dissociative recombination cross section of CD^+ and CH^+ molecular ions have revealed prominent resonances at low energy. They were assigned tentatively to capture into core-excited bound Rydberg states, electronically coupled both to the electronic initial continuum and to the dissociative final channel. We present here the result of calculations based on the multichannel quantum defect theory, using molecular data (quantum defects and electronic couplings) extracted from *ab initio* structure computations. In addition to the Rydberg states converging to the initial ground state $X\ ^1\Sigma^+$ of the ion, we calculated Rydberg series converging to the first two excited electronic states $a\ ^3\Pi$ and $A\ ^1\Pi$. The cross section convoluted with the experimental anisotropic Maxwell distribution presents a resonant structure very close to the experimental one, when the ion is assumed to be initially in the lowest rovibrational level of the ground state. We can thus assign the resonances observed near 0.3 and 0.9 eV to low vibrational levels of the $^2\Pi$ core-excited Rydberg states $(a\ ^3\Pi)5s\sigma$ and $(A\ ^1\Pi)3p\sigma$, respectively. We also give a theoretical estimate of the branching ratio for dissociation to various asymptotic limits, obtained by solving coupled equations for the nuclear wave functions of interacting $^2\Pi$ states of CH.

PACS number(s): 34.80.Lx

I. INTRODUCTION

Dissociative recombination (DR) of molecular ions is the most elementary reactive collision process, in which the kinetic energy of the incident electron is transformed into excitation of the core electrons:

$$AB^+ + e^- \rightarrow AB^{\ddagger} \rightarrow A + B^*, \tag{1}$$

where AB^+ is a diatomic or polyatomic ion, $AB^{\ddagger}$ denotes the excited ''molecular complex'' or transition state, and A and B^* are atomic or molecular fragments, in ground or excited states. DR occurs when the dominant configuration of $AB^{\ddagger}$ corresponds to a repulsive state and the chemical bond is eventually broken. Together with the repulsive states, bound states lying in the same energy range may be formed, leading to resonances in the DR cross section. They indicate a longer lifetime of the transient excited molecular complex and are the signature of the so-called ''indirect'' recombination process.

Most of the resonances previously observed or theoretically predicted in DR cross sections were narrow structures at low energy, hardly surviving the Maxwell average over electron velocities. They were assigned to excited rovibrational levels of bound Rydberg states with ground-state ion core, coupled to the initial ground-state electronic continuum by nonadiabatic interactions only. The main purpose of this paper is to identify another class of resonances, observed in TSR storage ring experiments, first on CD^+ [1], and then on OH^+ [2] and CH^+ [3]. They are broader and more prominent than the previous ones (see Fig. 1), and were tentatively assigned to capture into core-excited bound Rydberg states, electronically coupled both to the electronic initial con-

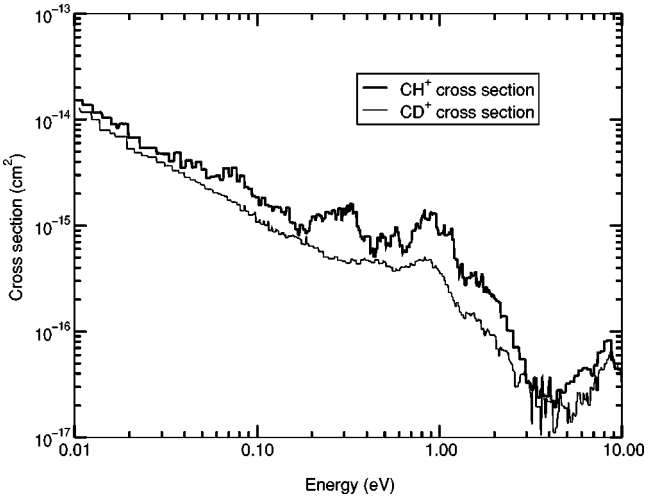

FIG. 1. The experimental cross sections of CH^+ and CD^+ dissociative recombination measured at TSR (Heidelberg) by Amitay *et al.* [3].

*Present address: Laboratoire de Photophysique Moléculaire, Université de Paris–Sud, 91405 Orsay, France. Permanent address: National Institute for Lasers, Plasma and Radiation Physics, Magurele 76900, Romania.

tinuum and to the dissociative final channel.

Following a previous rough simulation for this mechanism (see Ref. [4]), we present here the result of a more elaborate calculation of CD^+ and CH^+ DR at low energy. First, we performed multiconfiguration structure calculations for excited states of CH, to obtain a large set of bound Rydberg states with ground and excited ion cores. From these molecular data we extracted quantum defects and electronic interactions which were extrapolated above the ionization threshold to be used in the DR cross section calculation. This step is performed within the framework of the multichannel quantum defect theory (MQDT) including dissociative channels [7]. The usual procedure is here extended to include excited ion core states, with their vibrational structure and the relevant additional ionization channels. Such an extension has also been performed by Guberman [8] for the DR of N_2^+, but the resulting resonance structure was not discussed in detail.

Finally, we present the results of close-coupling calculations for the branching ratio between alternative dissociation limits, at low (0.1–0.3 eV) and higher (0.5–1.2 eV) energy. Although approximate, these results provide interesting information when compared to the measured branching ratios.

II. MOLECULAR CALCULATIONS

The CH radical was the first molecular species to be discovered in interstellar medium, in 1937 [9]. Four years later, the CH^+ ion was also identified in diffuse interstellar clouds, with large column densities [10]. In this environment with very low temperature and pressure, CH^+ may safely be assumed to be in its ground state, and, due to relatively high electron densities, the main destruction process is the dissociative recombination, which results in neutral fragmentation

$$CH^+(X\ ^1\Sigma^+, v=0)+e^-\rightarrow CH^{\ddagger}(^2\Lambda)\rightarrow C^*+H(1s). \quad (2)$$

This process has been studied repeatedly over the years, both experimentally [11] and theoretically [12–15], because the fast DR rate usually accepted (about $10^7\ cm^3\ s^{-1}$ at 100 K) makes it difficult to understand the large CH^+ abundance observed, and thus the following astrochemistry of various related species.

A helpful feature for a fast low-energy DR rate is the existence of a dissociative state of the neutral whose potential curve crosses the ion ground-state curve close to the Franck-Condon region of the $v=0$ level. The best candidate in the case of CH is the $2\ ^2\Pi$ state, namely, the higher of the two $^2\Pi$ states going to the $C(^1D)+H(1s)$ asymptotic limit, with main configuration $(1\sigma^2 2\sigma^2 3\sigma 1\pi 4\sigma)$. The most recent multiconfiguration calculation by Takagi *et al.* [15] found that its potential curve crosses that of the ion ground state near the inner turning point of the $v=1$ level, which leads to a non-negligible overlap between the low-energy dissociative wave function and the $v=0$ vibrational function. This feature, together with a substantial electronic coupling between this doubly excited state and the ground-state ionization continuum, leads to a relatively fast DR rate ($1.2\times10^{-7}\ cm^3\ s^{-1}$ at 120 K) for cold CH^+.

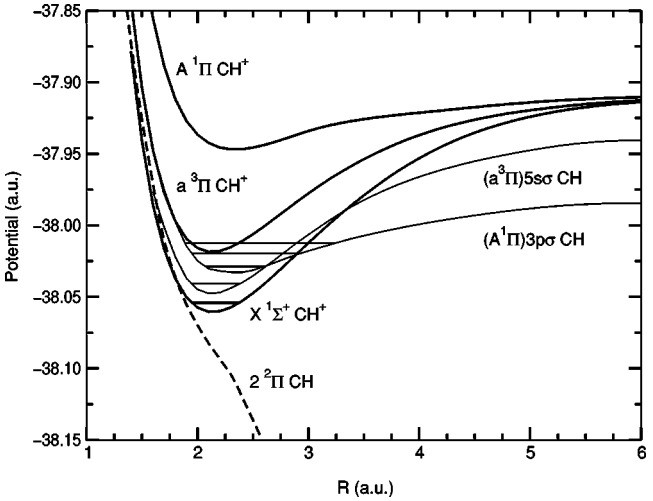

FIG. 2. Potential curves of CH^+ (the ground state $X\ ^1\Sigma^+$ and the first two excited states $a\ ^3\Pi$ and $A\ ^1\Pi$, with thick solid lines [16]) and of CH (the $2\ ^2\Pi$ dissociative curve, with dashed line [15], and two Rydberg states with excited ion cores with thin solid lines). The vibrational levels that are involved in the formation of the large resonances shown in Fig. 1, are also represented. The data points for the dissociative curve of CH have been communicated by Takagi.

In the present paper we do not reexamine the relative positions of the dissociative and the ion potential curves, which would require a high precision calculation, both for the ion and neutral molecule. In our MQDT treatment of dissociative recombination, we use the potential curves of Green *et al.* [16], for the ground state ($X\ ^1\Sigma^+$) and the next two excited states ($a\ ^3\Pi$ and $A\ ^1\Pi$) of the CH^+ ion (Fig. 2). For the $2\ ^2\Pi$ dissociative state of CH we used the data of Takagi *et al.* [15], which were calibrated to the ion ground state of Green. Since there was a lack of molecular data for high Rydberg states of CH, we carried out a set of molecular structure calculations, in order to locate core-excited Rydberg states, and to determine their couplings with other Rydberg or valence states, important for the dissociative recombination.

Low-energy DR of CH being mainly driven by the $2\ ^2\Pi$ dissociative state, we restrict our computations to molecular states of symmetry $^2\Pi$. Indeed, rotational effects have been shown to play a minor role in dissociative recombination, at least for total DR cross sections [17]. The effect of the rotational coupling between states of different symmetry, on the branching ratios of the final products, might however be important. This aspect will be discussed in Sec. IV C.

The calculations are performed with the MESA package of programs developed by Lengsfield III *et al.* [18], using Gaussian-type orbitals. For each internuclear separation R, the orbitals are determined by a multistep procedure, designed to provide Rydberg states with high principal quantum number. In the first step, we obtain valence orbitals from a multiconfiguration self-consistent field (MCSCF) calculation, with the ground and the next two excited states of CH^+ ($X\ ^1\Sigma^+$, $a\ ^3\Pi$, and $A\ ^1\Pi$). The atomic bases used are the triple zeta bases of Dunning [19] ([$9s5p1d/5s3p1d$] for C,

and $[4s1p/3s1p]$ for H). In the next step we calculate natural orbitals starting from the first seven lowest states of the neutral molecule. The basis of natural orbitals is expanded afterwards by the inclusion of several diffuse orbitals: 2 *s*-type (with exponents 0.04 and 0.012), 7 *p*-type (exponents 0.08, 0.05, 0.03, 0.01, 0.005, 0.002, and 0.001), and 2 *d*-type (exponents 2.0 and 0.1) orbitals centered on the C atom. The final basis is formed from 32 σ orbitals, 28 π orbitals, and 3 δ orbitals. Last, we perform a CI calculation with a selected set of configurations. The 1σ orbital is considered always fully occupied. Four other electrons occupy valence orbitals (2σ, 3σ, 4σ, and 1π), while the last remaining electron may be either a valence or a Rydberg electron. The total number of configurations included in the CI calculation is 1368.

At each internuclear distance we calculated the lowest 35 roots of the Hamiltonian matrix. By analysis of the configuration of the states, we identified five Rydberg series converging to the lowest three states of CH^+, with at least four consecutive members each. On the basis of their leading configuration, they can be designated as $(X\ ^1\Sigma^+)np\pi$, $(a\ ^3\Pi)ns\sigma$, $(a\ ^3\Pi)np\sigma$, $(A\ ^1\Pi)ns\sigma$, and $(A\ ^1\Pi)np\sigma$. It is worth noting, however, that the *l* quantum number of the external orbitals is only indicative, the Rydberg orbitals being subject to *l* mixing induced by the anisotropy of the molecular potentials [15,20]. Our CI basis did not include enough diffuse orbitals of *d* type to provide the $(X\ ^1\Sigma^+)nd\pi$ Rydberg series, shown by Takagi [15] to display mixing with $(X\ ^1\Sigma^+)np\pi$ series. We did not include either the *l* mixing of the excited core Rydberg series into the MQDT calculations, our purpose being only to identify the dominant character of the broad resonances that appear in the experimental cross sections.

The potential curves obtained in the CI calculation are adiabatic, and display avoided crossings. The quantum defects corresponding to these potentials will show their adiabatic character by large variations near the avoided crossing points. Since the MQDT treatment of DR is based on a quasidiabatic representation [21], we need a set of *smooth* quantum defects which do not include Rydberg-valence mixing. To achieve that we adopt a simple procedure based on an idea of O'Malley [22]. We define a subset of the total set of configurations, consisting of Rydberg configurations with given symmetries for the ion core and the outer electron. The CI calculations performed with the restricted subset provide quasidiabatic Rydberg states, not mixed with the valence states. To determine the quantum defects, we use the molecular Rydberg formula for the energy $E_{nl\lambda}$ of a state with external orbital $nl\lambda$ (l and λ are the quantum numbers of the orbital momentum and of its projection on the internuclear axis for the Rydberg electron):

$$E_{nl\lambda}(R)=E_{\rm ion}(R)-\frac{1}{2[n-\mu_{l\lambda}(R)]^2}. \tag{3}$$

We obtain by extrapolation the energy $E_{\rm ion}$ of the ion state (as the Rydberg series limit), and from it an accurate quantum defect function for each Rydberg series. In Fig. 3 we show the quantum defects of the Rydberg series that were included into calculation. The ion limits obtained by extrapolation of the $ns\sigma$ and $np\sigma$ Rydberg series with the same excited core agree within 0.001 a.u. (0.027 eV).

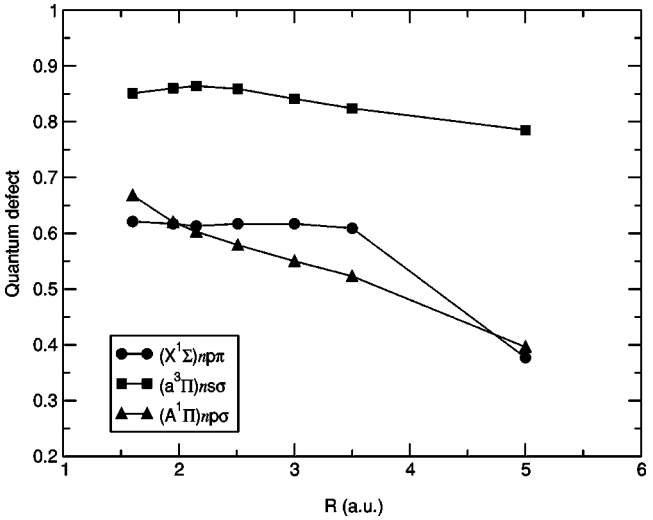

FIG. 3. Quantum defects of the Rydberg series included in the MQDT calculation.

Table I shows an example illustrating our method. One can see here the effective quantum numbers n^* of four consecutive states of the $(X\ ^1\Sigma^+)np\pi$ Rydberg series identified in CI results, and the $\mu_{p\pi}(R)=n-n^*$ quantum defect of the series. The quantum defect depends weakly on the principal quantum number *n*, and the lowest state shows the largest deviation compared to the rest of the series. The quantum defect of a series, to be used in the MQDT computations, can be defined as the limit in the adjoining continuum of the quantum defect at the ionization threshold. However, since the energy of the more excited states is less accurate, due to the limited size of our configuration set, the quantum defect of the high *n* Rydberg states is determined with less precision. For this reason, the quantum defect we assign to a series (e.g., the last column of Table I) is not that of the highest Rydberg state identified in our CI results, but the average of the quantum defect over all the states of the series. We treat similarly all identified Rydberg series.

In the quasidiabatic representation, the $2\ ^2\Pi$ dissociative state of CH will be described by its dominant configuration $1\sigma^2 2\sigma^2 3\sigma 1\pi 4\sigma$. To calculate the strength of the interaction between the Rydberg states and the dissociative state, we add the dissociative configuration to the various subsets of Rydberg configurations, and perform CI computations with the new subsets of configurations obtained in this way. The Rydberg states we thus determine are shifted from their position in the preceding computations. The shifts are induced by Rydberg-valence interaction, and they may be used to calculate the interaction strength. Because they are small compared to the distances to the next upper or lower Rydberg states, for small *n* values, we treat each shift independently. We can thus apply a simple 2×2 deperturbation formula to calculate the coupling $V_{n_i d}$, between a given n_i Rydberg state and the dissociative state *d*, with *i* indexing the Rydberg series.

The scaled interactions

TABLE I. The effective quantum numbers n^* of four successive Rydberg states of the series $(X\ ^1\Sigma^+)np\sigma$ and its average quantum defect $\mu(R)$ (see text).

R(a.u.)	$n^*(1)$	$n^*(2)$	$n^*(3)$	$n^*(4)$	$\mu(R)$
1.60	2.370	3.387	4.384	5.374	0.621
1.95	2.375	3.391	4.389	5.379	0.617
2.15	2.378	3.394	4.392	5.383	0.613
2.51	2.375	3.391	4.389	5.379	0.617
3.00	2.375	3.391	4.388	5.379	0.617
3.50	2.383	3.398	4.396	5.387	0.609
5.00	2.628	3.623	4.613	5.628	0.377

$$\tilde{V}_{n_i d}(R) = \sqrt{\frac{n_i^{*3}}{2\mathrm{Ry}}}\, V_{n_i d}(R), \tag{4}$$

are practically independent of n_i (as expected for successive states of a Rydberg series), and we obtain our coupling function $V_{id}(R)$ by averaging over all the values $\tilde{V}_{n_i d}(R)$. In the equation above, Ry is the Rydberg energy. The couplings $V_{id}(R)$, shown in Fig. 4, will be used as input data for our MQDT treatment of the dissociative recombination (see Sec. III). Note that the values we obtain for the scaled coupling of the $(X\ ^1\Sigma^+)p\pi$ with the dissociative $2\ ^2\Pi$ state is about twice the coupling of Takagi [15] at the two R values where we can compare.

The other coupling functions needed, $V_{ij}(R)$, between different ionization channels i and j are dimensionless, and can be obtained similarly by an average over terms of the form

$$\tilde{V}_{n_i n_j}(R) = \frac{n_i^{*3/2} n_j^{*3/2}}{2\mathrm{Ry}}\, V_{n_i n_j}(R). \tag{5}$$

If i and j are series with the same ion core, the coupling functions are identically zero. To determine the $V_{n_i n_j}$ coupling elements, a method similar to that described above is applied. Now, instead of a Rydberg series interacting with the dissociative state we have two interacting Rydberg series. The problem is complicated by the fact that, even treating each shift independently, this shift is the result of several interactions. To calculate the coupling function between two series, we take the first state from each series, and treat their shifts as being the result of a two-state interaction. The coupling element we obtain is corrected for the contribution of the other states, with a factor estimated on the basis of the scaling law (5). The same law yields us, finally, the coupling function $V_{ij}(R)$. Another difficulty we encounter is the intermingling of the Rydberg states of the two series. Certain states may be subject to opposite influences from the neighboring states, in this case the shift being no longer a measure of the interaction strength. Finally, in our approach, all the series with the same core appear together in the CI results. Since we find one series with ground ion core and two series for each excited core, the coupling elements between the excited core Rydberg states are very difficult to obtain by this method, only an estimation of their strength being possible. These last couplings, however, have little influence on the resonance feature we are studying, and have been put to zero for the present DR computations. Overall, the precision in determining the $V_{n_i n_j}$ coupling elements is poorer than for the $V_{n_i d}$ coupling elements. The coupling functions we obtain are shown in Figs. 4 and 5.

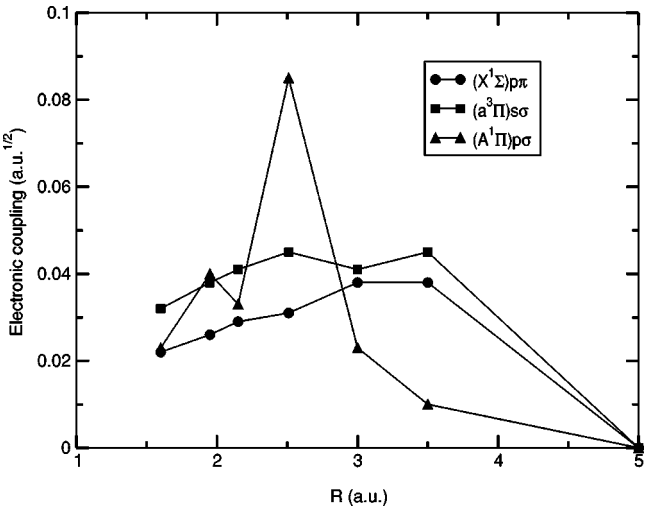

FIG. 4. Rydberg-valence coupling functions between Rydberg series with different ion cores and the $2\ ^2\Pi$ dissociative state [see Eq. (4)].

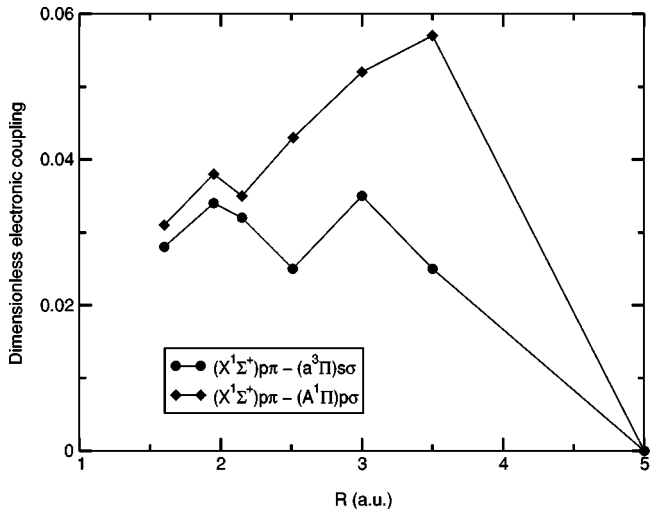

FIG. 5. Rydberg-Rydberg coupling functions between Rydberg series converging to different ion states [see Eq. (5)].

III. CROSS-SECTION CALCULATIONS

To calculate the DR cross section for CH^+ and CD^+, initially in their ground states, we use the multichannel quantum defect theory (MQDT), which was designed to handle Rydberg resonances. Recent review papers [4–6], summarize the extension of MQDT to DR [7] and report on various applications. Here we will just describe how the core excited bound states are included in the calculations and comment on the resonance structure they induce in the cross section.

The MQDT approach to DR is based on mixing two types of channels: (i) the dissociation channels, associated with electronic states of the neutral molecule which are open for dissociation in the energy range of interest and (ii) the ionization channels, each of them associated with a given threshold, defined as a (ro)vibrational level of an ion electronic state, and with a given partial wave (or Rydberg orbital) of the external electron. The ionization channels will be labeled by (i,v_i) where i stands for the ion electronic state and v_i for the vibrational level in the ion potential. The molecular ion is assumed to be initially in the ground rotational level, and we neglect any rotational excitation. Some calculations will test the effect of initial rotational excitation, but we will simply add the same centrifugal term in all the molecular potentials involved.

What we add here, with respect to previous MQDT calculations of DR processes, is a set of ionization channels built on excited electronic states of the ion, and not only on the ground state, as previously. The channel thresholds for various electronic cores are the successive vibrational levels of the corresponding ion states. They have to be ranked according to their energy, which requires care when the different vibrational structures overlap.

The most important feature of these additional ionization channels is that they correspond to doubly excited configurations, and are directly coupled via electronic interaction to the entrance channel $[AB^+(X)+e]$, and not only by weak vibrational interactions as the ionization channels built on the ground-state ion core. Consequently, the resonances attributed to the capture of the incoming electron into Rydberg states associated with these core-excited channels may appear as relatively broad peaks, instead of the narrow resonances mostly in form of dips, characteristic of the Rydberg states with ground state ion core.

The building blocks for this type of indirect mechanism are the electronic interaction matrix elements

$$V_{v_i v_j} = \int \chi_{v_i}(R) V_{ij}(R) \chi_{v_j}(R) dR, \tag{6}$$

where $V_{ij}(R)$ is the electronic coupling function between the two Rydberg configurations, determined by Eq. (5), and $\chi_{v_i}(R)$ and $\chi_{v_j}(R)$ are bound vibrational wave functions associated with these two ion states. They enter in the interchannel interaction matrix as off-diagonal terms, and can be relatively large if the two core state geometries allow for large overlaps between some of their vibrational levels. Other additional matrix elements are $V_{v_i d}$, responsible for the predissociation of the core excited bound Rydberg states which completes this indirect DR process

$$V_{v_i d} = \int \chi_{v_i}(R) V_{id}(R) F_d(R) dR, \tag{7}$$

where F_d is the continuum nuclear wave function in the dissociative channel. For simplicity we assume here that a single dissociative channel d is active, but several dissociation channels may be easily handled in the same calculation.

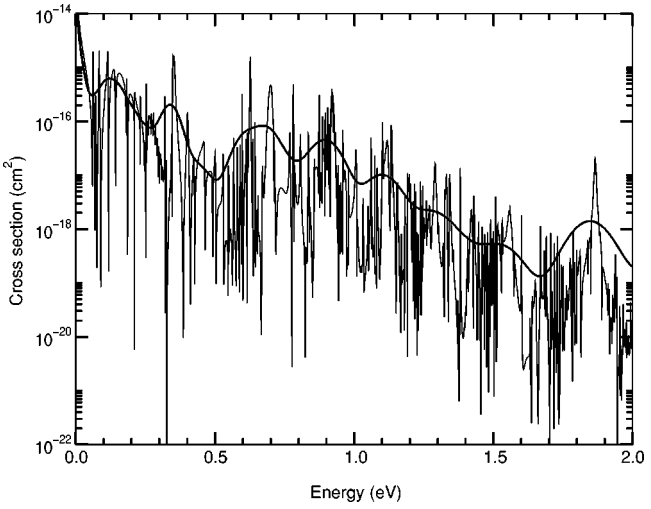

FIG. 6. The calculated cross section of CH^+ dissociative recombination, before (thin line) and after (thick line) convolution with the anisotropic Maxwellian distribution of electron energies given in Ref. [3]. The transversal temperature is $kT_\parallel = 1$ meV and the longitudinal one $kT_\perp = 17$ meV.

These matrix elements, together with the terms $V_{v_0 d}$ which connect directly the entrance channel to the dissociative one, are used to build the electronic reaction matrix K. We use a perturbative expansion of the Lippman-Schwinger equation to get K, restricted here to the first order where K is simply equal to V, the electronic interaction matrix. The K matrix is then diagonalized and the resulting eigenchannels are mixed by vibrational interactions, using the frame-transformation scheme of molecular MQDT [23]. In the last step, closed ionization channels, i.e., channels with threshold energies higher than the current total energy, are eliminated at long range, which leads to the scattering matrix S restricted to open channels. The DR cross section is finally obtained from the matrix element $|S_{v_0 d}|^2$, including the resonance structure due to bound Rydberg states in the closed channels.

The present calculations, restricted to the $^2\Pi$ symmetry (see Sec. II), include a total of 52 ionization channels for CH^+, associated with the 22 vibrational levels of the ground state $X\ ^1\Sigma^+$ and the 18 and 12 levels of excited states $a\ ^3\Pi$ and $A\ ^1\Pi$, respectively. This number increases to 68 for CD^+, due to the smaller vibrational spacing.

IV. RESULTS AND DISCUSSION

A. Results for CH^+

The total DR cross section for CH^+ ion is shown in Fig. 6, for ions initially in the lowest rovibrational level of the ground state electronic state. Since our interest is in the low-energy core-excited resonances, the energy in our calculations is restricted to the range 0.001–3 eV. Beyond 3 eV, other dissociative states, besides the $2\ ^2\Pi$ state, become active, as one can guess from the broad peak in the experimental cross section at $\approx$9 eV [3]. The complicated structure of the cross section is the signature of strongly overlapping

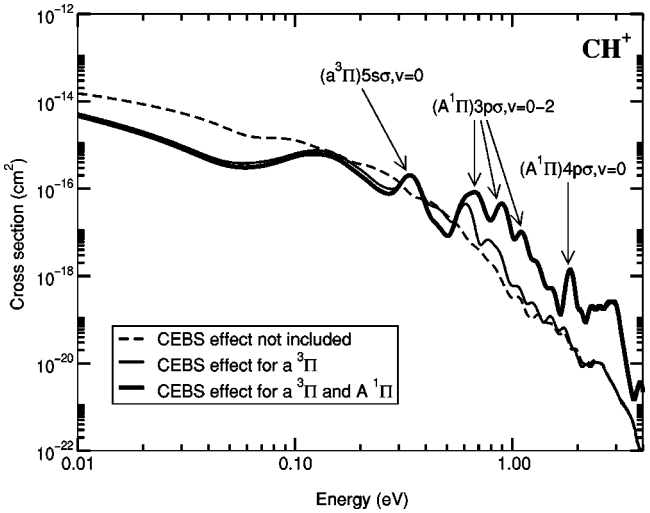

FIG. 7. The effect of Rydberg series with excited ion cores. Comparison between convoluted CH^+ dissociative recombination cross sections, calculated with the inclusion of different numbers of core excited bound Rydberg series (CEBS).

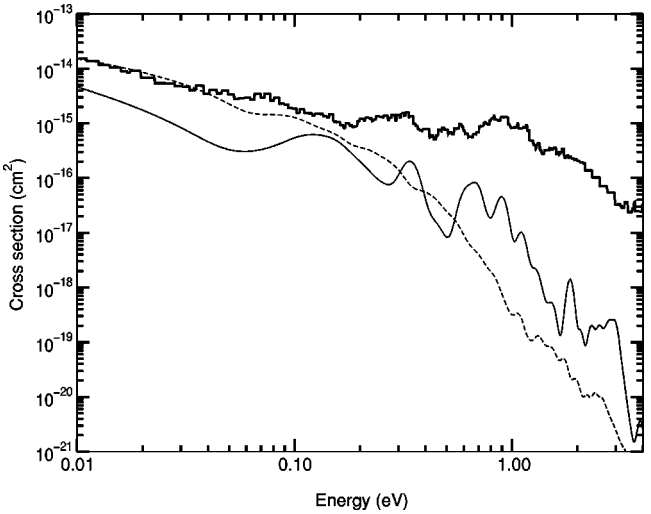

FIG. 8. Comparison between calculated cross-section (thin lines) and the experimental results (thick line), for the dissociative recombination of CH^+ ground states. The solid thin line represents the result with all three lowest bound states of CH^+ included in the calculation, while the dashed thin line represents the cross section when only the ground ion state of CH^+ is included.

resonances, due to electron capture into various bound Rydberg states, with ground or excited ion core. A clearer picture emerges once the theoretical results are convoluted with the experimental anisotropic Maxwell distribution given in Ref. [3], as it is shown in Fig. 6. The numerous narrow and closely lying resonances, due to vibrational capture into high n Rydberg states with ground-state ion core, are partly washed out in the convolution process, and only the more substantial core-excited resonances survive. The convoluted cross section, shown with thick solid line in Fig. 7, presents a resonance structure very similar to the experimental one, although lower in magnitude. We assigned these resonances by analysis of our MQDT calculations.

To perform this analysis, we made test calculations with an increasing number of closed ionization channels. The dashed line in Fig. 7 shows the convoluted cross section obtained with only the ion ground state included, hence only Rydberg series converging to vibrational levels of the ion ground state. No prominent structure appears. The landscape begins to change when the $a\ ^3\Pi$ core state is introduced in the calculation, as shown by the thin solid line in Fig. 7. By varying the number of vibrational levels introduced into the calculation, we have been able to assign the two peaks which survive the convolution near 0.3 and 0.6 eV to the two lowest vibrational levels of the $(a\ ^3\Pi)5s\sigma$ Rydberg state. Finally, adding the $a\ ^1\Pi$ core state into the calculation leads to the thick solid line, with new resonances in the energy region 0.6–1.2 eV. They can be assigned to the $v=0-2$ levels of the $(A\ ^1\Pi)3p\sigma$ Rydberg states, although they clearly overlap and interfere with the higher of the two previous resonances with a $a\ ^3\Pi$ core. The effect extends until almost 2 eV due to weaker capture in the following vibrational levels of the same Rydberg state, and at about 1.8 eV the resonances due to $(A\ ^1\Pi)4p\sigma$ begin to appear, followed by traces of the $(A\ ^1\Pi)5p\sigma$ series above 2.3 eV. It is worth noting that including these two sets of closed ionization channels associated with the excited ion core states not only induces the strong resonance structure of the cross section, but affects the magnitude of the cross section even away from resonances, through channel mixing effects. In this particular case the effect is mostly destructive at very low energy where the cross section drops by about a factor of 4 when the two excited cores are included, probably due to increased autoionization, but it is strongly constructive in the resonance region.

We have checked that the same calculation for initial $v=1$ vibrational level of CH^+ ground state leads to a similar resonance structure but at lower energy, clearly not in agreement with experiments. This confirms the vibrational relaxation of the CH^+ ions in the beam, after 15–20 s storage time, as expected from the vibrational lifetime of about 5 μs.

In Fig. 8 we present a comparison between the experimental cross section and our theoretical results. Together with the result of a calculation including all three lowest bound states of CH^+, we show the DR cross section obtained when the $a\ ^3\Pi$ and $A\ ^1\Pi$ excited states are omitted (dashed thin line, as in Fig. 7). This curve lies almost on top of the experimental cross section at low energies, and agrees with the cross section of Takagi, obtained with the $X\ ^1\Sigma$ core only [15] (the additional capture due to the d wave in Takagi's results is compensated by our larger coupling for the p wave, see Sec. II). However, including the core excited closed channels reduces the cross section in this region, as already noted on Fig. 7.

Several reasons may explain the fact that our computed cross section is smaller than the experimental one, by almost an order of magnitude in some energy ranges. First, we have neglected the contribution of the d wave of the recombining electron, which was shown by Takagi [15] to be smaller than the p-wave contribution but non-negligible. Second, we will see later (in Sec. IV C) that some $^2\Sigma^+$ Rydberg states, not included in our calculation, could contribute to the cross sec-

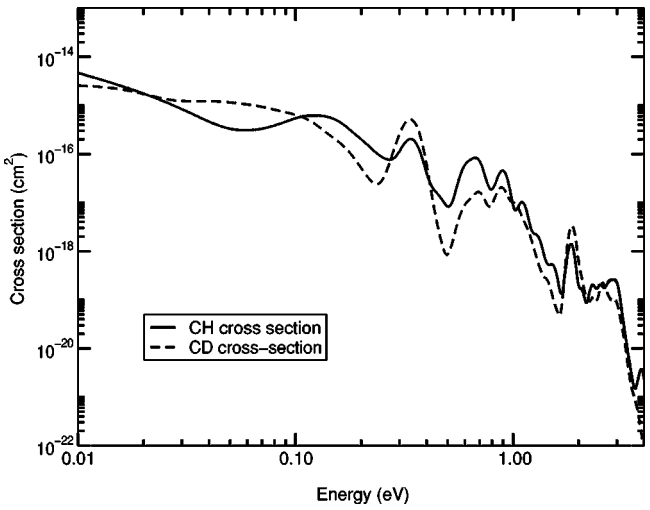

FIG. 9. Isotopic effect. Convoluted theoretical cross-sections for ground state CH^+ (solid line) and CD^+ (dashed line) dissociative recombination.

tion by about 20% through nonadiabatic interactions. Finally, it is worth noting that any small translation upwards of the $2\ ^2\Pi$ dissociative curve induces a large increase of the total cross section, because this curve lies in the classically forbidden inner region for the $v=0$ vibrational wave function of the ground-state ion. In particular, a shift upwards of this curve by 0.2 eV (0.008 a.u.), which is the accuracy claimed in Ref. [15], would increase the cross section by about a factor 3 at low energy, leading to a better agreement with the experiment in this region.

Another feature to be discussed in our results is the resonance at 1.8 eV, that we assigned to the $(A\ ^1\Pi)4p\sigma$ Rydberg series. In the experiments there is no prominent resonance peak in that region. This can be due to missing channels in our calculations, either Rydberg series or dissociative states, which might mask this resonance. Note that in this region the difference between the measured and the computed cross sections becomes larger than at 1 eV, suggesting that contributions from new states which open to dissociation are missing from our computations. On the experimental side, the statistics is weaker in this energy range than at smaller energies, leading to a lower-energy resolution, which can prevent the resonance structure to appear clearly.

B. Isotopic effect

In Fig. 9 we compare the cross sections obtained for the two ground state ions CH^+ and CD^+ using exactly the same approach and the same electronic data. The figure shows that the resonance structure of the cross section for the two isotopes are very similar. At very low energy, the CD^+ cross section is somewhat smaller, which can be explained by the fact that the $v=0$ vibrational level of CD^+ is deeper in the potential well than for CH^+, leading to a smaller Franck-Condon factor. The resonance at 0.3 eV displays no visible isotopic shift because it is formed with the participation of the $v=0$ vibrational level of the $a\ ^3\Pi$ core, and the differences in energy between the ground vibrational levels of all three cores involved in our calculations display practically no isotopic effect. On the other hand, the resonances attributed to $v\neq 0$ vibrational levels display a small shift towards smaller energy for CD^+, as it is expected.

The experimentally measured CD^+ cross section displays no resonance at 0.3 eV (see Fig. 1). However in these measurements CD^+ could have been not fully vibrationally relaxed [3], due to a longer lifetime of the excited levels than for CH^+, and this may reduce the resonance peak due to an average effect. Note also that the CD^+ cross section is relative, the ion beam current being too weak to determine the total number of ions in the ring, and it is adjusted at low energy to match that of CH^+. On the theoretical side, we did not include in the calculation all the Rydberg series which might contribute to the total DR cross section. This could make the main resonance peak more prominent than it really is. However, we think that even in a more complete calculation the isotopic effects on the core-excited resonance structure should be small, since this is dominated by electronic interactions.

C. Branching ratios

In addition to total cross sections, the TSR experiment on CH^+ measured branching ratios between asymptotic products of the DR process for selected energies of the incident electron, using a 2D imaging detector. The observed distributions of product states differ for the two energy regions around the core-excited resonances that we analyze in this paper. Around 0.28 eV, only three asymptotic limits are open: $H(1s)+C(^3P)$, $C(^1D)$, $C(^1S)$ and the branching ratio (see Table I of Ref. [3]) is about 75% to the second limit $C(^1D)$, 25% to the higher one $C(^1S)$. At 1.18 eV only 10% of the products go to these two low limits, while 90% are distributed among three newly open limits, corresponding to the excited states $C(^3P^0)$, $C(^1P^0)$, and $C(^3D^0)$.

This distribution among accessible dissociation limits results from various types of couplings between the ''doorway'' $2\ ^2\Pi$ state accessed by electron recombination and other dissociative states of the neutral molecule CH. This process is closely related to the multichannel photodissociation process of CH thoroughly studied by E. van Dishoeck [24], who performed a SCF-CI calculation of most excited states of CH in a broad energy range below the ionization threshold.

Selecting from this study the relevant potential curves and couplings, the transition probabilities among interacting states on the way to dissociation have been estimated by using the Landau-Zener formula [25], as applied recently by Urbain *et al.* [26] to the DR process of HD^+, or by performing a close-coupling calculation of the branching between the dominant molecular states.

1. Branching ratio in the 0.3 eV energy region

The low-energy branching has been assumed [3] to result from a nonadiabatic transition between the $2\ ^2\Pi$ state which correlates to the $C(^1D)+H(1s)$ limit, and the $2\ ^2\Sigma$ state which is the only state leading to the limit $C(^1S)+H(1s)$. The rotational coupling between these two states has been

evaluated by van Dishoeck [24] from multiconfiguration wave functions. The Landau-Zener formula gives the probability to jump from one state to the other:

$$p = 1 - e^{-2\pi\gamma}, \tag{8}$$

where the exponential factor γ is given by (see Ref. [25]):

$$\gamma = \frac{V_{12}^2}{\hbar v_R \{d/dR[V_{11}(R) - V_{22}(R)]\}}. \tag{9}$$

V_{12} is the coupling value at the crossing point $R = 3.5$ a.u. between the two states, and $V_{11}(R)$ and $V_{22}(R)$ are the energy of the two intersecting states. We obtain a probability almost unity to stay on the $^2\Pi$ dissociative state, while the experiment measured a branching of almost 25% to the higher $^2\Sigma$ curve leading to the C(^1S) limit.

We then checked our Landau-Zener result by solving a system of two coupled equations involving the $2\ ^2\Pi$ and $2\ ^2\Sigma^+$ electronic states and the rotational coupling function given in Ref. [24]. The transition probability from $2\ ^2\Pi$ to $2\ ^2\Sigma$ extracted from the scattering matrix associated with the full collision along these two states is very small, of the same order of magnitude (10^{-4}) as the Landau-Zener result. As the error bar of the measurement at 0.28 eV is large (25% $\pm$25%, see Table I of Ref. [3]) we extended the close-coupling calculation to the lower energy region ($\approx$0.1 eV) where the measured branching ratio is 21%$\pm$10%. Again, the calculated value was found much smaller.

Clearly, the rotational coupling is too small to be responsible for the observed 25% branching to the higher C(^1S) limit. The flux going to the C(^1S) limit probably results from another mechanism, which should proceed through direct capture into the manifold of $^2\Sigma$ states. As no dissociative valence state with this symmetry has been found in the relevant energy range, this mechanism has to proceed through nonadiabatic capture into the $^2\Sigma$ Rydberg states built on the ion ground state. Radial non-Born-Oppenheimer interactions have been proved in other cases (e.g., HeH^+ [27]) to be effective for the dissociative recombination in the absence of substantial electronic interaction. Here the electronic mechanism through the $^2\Pi$ valence state is still responsible for the bulk of the DR cross section, but a small contribution of nonadiabatic interactions could be enough to explain the observed branching ratio, without affecting drastically the total cross section. A quantitative check of this assumption would require the calculation of nonadiabatic couplings which is beyond the scope of this article, centered on electronic processes responsible for the core-excited observed resonances.

2. Branching ratio in the 1 eV energy region

The situation becomes more complex at higher energy where more dissociation limits are open. If we restrict ourselves to the $^2\Pi$ symmetry, at a collision energy of 1 eV we have to consider three more open asymptotic limits H($2s$) + C(^3P), C(^1P), and C(^3D) (see Fig. 10) which have been found to attract about 90% of the dissociation flux at sample energies around 1 eV, namely, 0.93, 1.04, and 1.18 eV [3]. The first two correspond to Rydberg states of the carbon atom, with the same configurations $1s^2 2s^2 2p(^2P)3s$ and parallel (^3P) or antiparallel (^1P) spins for the $2p$ and $3s$ electrons. Spin considerations lead to the correlation of the $(A\ ^1\Pi)3s\sigma$ molecular Rydberg state to the lower C(^3P) limit, and of $(a\ ^3\Pi)3s\sigma$ to the higher C(^1P) state.

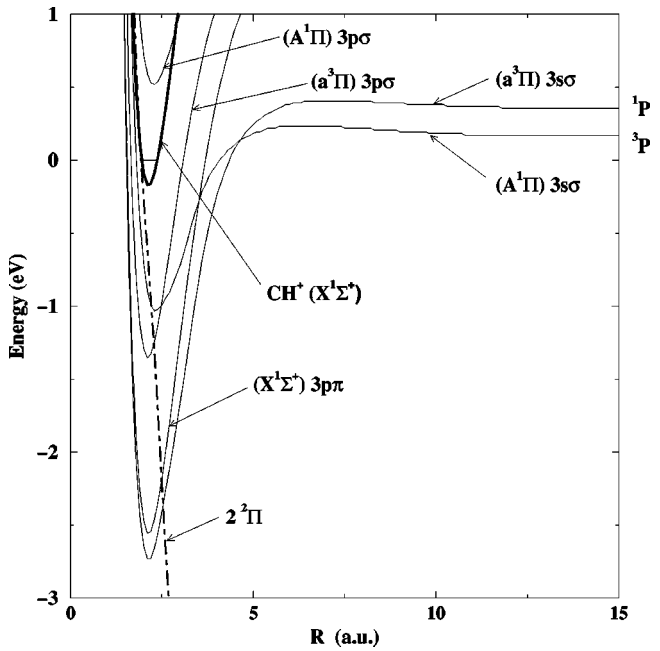

FIG. 10. Some of the potential curves involved in the close-coupling calculation of the branching ratios (see text).

The third limit accessible for $^2\Pi$ molecular states in this energy range, C(^3D), corresponds on the contrary to a doubly excited configuration C($1s^2 2s 2p^3$) and is the limit of a steep dissociative electronic state with principal configuration $1\sigma^2 2\sigma 3\sigma^2 1\pi 4\sigma$. In our *ab initio* molecular calculations we could identify this highly excited state at large internuclear distance only (around 3.5–5 a.u.). It clearly plays a very minor role in the recombination step for ground state CH^+, and it is most probably populated by redistribution of the flux from $^2\Pi$ Rydberg states (still closed for dissociation) that are crossed at large distance.

Since we could not obtain reliable energies and couplings for this long range dissociative state, we decided to restrict our branching ratio calculations to a limited aim. We checked the transfer of population flux from the lowest C(^1D) dissociation limit to the higher C(^3P) and C(^1P), knowing that their branching ratios will be overestimated, because part of the flux is redirected toward the still higher C(^3D) limit. Even for this limited aim, a Landau-Zener calculation involving only the lowest three $^2\Pi$ molecular states open for dissociation around 1 eV would not be very reliable, since there are also many bound $^2\Pi$ Rydberg states in the same energy range, that undergo several crossings with the dissociative state (see Fig. 2).

We thus decided to perform a close-coupling calculation involving, besides the dissociative valence state $2\ ^2\Pi$, five series of $^2\Pi$ Rydberg states, with main configurations $(X\ ^1\Sigma^+)np\pi$, $(a\ ^3\Pi)ns\sigma$, $(a\ ^3\Pi)np\sigma$, $(A\ ^1\Pi)ns\sigma$, and $(A\ ^1\Pi)np\sigma$, respectively, and principal quantum numbers

$3 \leqslant n \leqslant 7$. Only the lowest state $(3s\sigma)$ of each core-excited series is open for dissociation but the higher bound states may be coupled to them by the electronic interactions $V_{n_i n_j}$ evaluated in Sec. II [see Eq. (5)], and also to the $2\ ^2\Pi$ dissociative state. The Rydberg potential curves are either known from the *ab initio* calculations of Sec. II, or (for higher n values) deduced from the ion curve by means of the quantum defect functions [Eq. (3)]. At long distance we simply correlate them diabatically to the corresponding Rydberg states of carbon.

The present close-coupling calculation treats the DR process as a half collision, the capture into various electronic states being described just by the source terms

$$\langle \chi_0^+ | V_{el} | F_{d_i} \rangle, \tag{10}$$

where χ_0^+ is the bound vibrational function in the initial state of the molecular ion, F_{d_i} is the nuclear continuum wave function for the dissociative state i, and V_{el} the electronic coupling between the initial ion ground state and the i dissociative state. We performed two sets of calculations, one in which all the doubly excited electronic states in our model were allowed to directly capture the incoming electron, and the other one with only the $2\ ^2\Pi$ state directly coupled to the continuum, as in the MQDT calculations described in Sec. III. On the other hand, we neglected here the short range autoionization back to the electronic continuum, which on the contrary was properly included in the MQDT treatment.

The approximate partial cross sections thus obtained were convoluted with the anisotropic Maxwellian distribution specific to the experimental measurements [3]. From the convoluted cross sections we could estimate the branching ratios shown in Fig. 11, in full line for the case of source terms in all $^2\Pi$ states and in dashed line when direct capture is allowed in the $2\ ^2\Pi$ dissociative state only. As we go up in energy the branching ratio for $C(^1D)$, which represents the atomic limit of the $2\ ^2\Pi$ state, falls down from 100% to less than 10% as the ^1P limit is reached. The branching ratio for each new open limit, $C(^3P)$ and then $C(^1P)$, oscillates around a mean value of about 0.6 for $C(^3P)$, and 0.3 for $C(^1P)$. Both are certainly overestimated in this approximate treatment which does not allow for dissociation into the higher $C(^3D)$ limit, that opens up 0.26 eV above $C(^1P)$. Nevertheless, we agree with the observation that less than 10% of the flux still goes to the lowest $C(^1D)$ limit. A more sophisticated calculation of branching ratios should properly connect the short range MQDT treatment to the close-coupling calculation, and would need further calculations of highly excited states. However, from this preliminary study we can draw some conclusions which will help for a later more complete calculation.

(i) At least for the capture due to electronic interactions, the $2\ ^2\Pi$ state seems to still play the dominant role as a doorway state for DR in the 1 eV energy region: allowing for direct capture into the other core-excited Rydberg states (full line in Fig. 11, to be compared with the dashed line results) has very little effect on the branching ratios. This is mainly due to smaller electronic couplings with the initial electronic

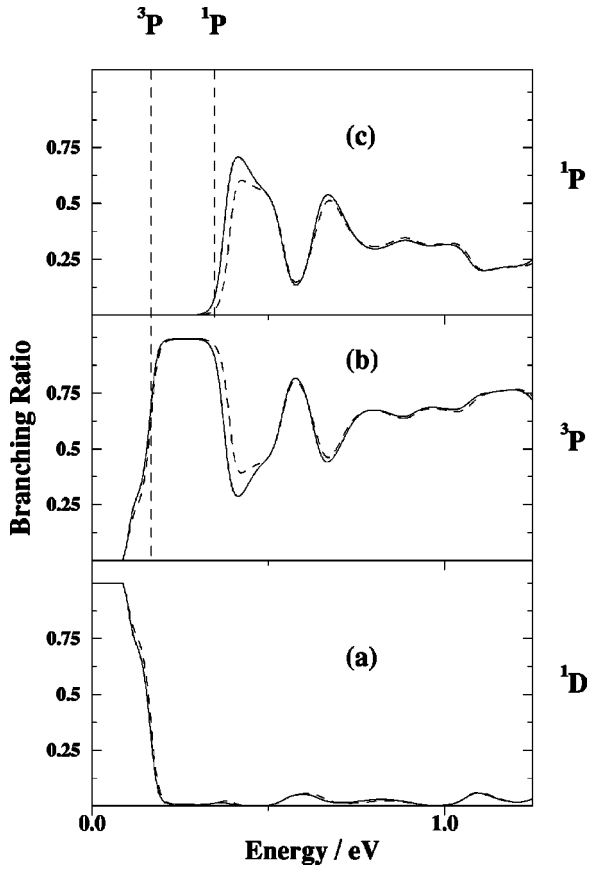

FIG. 11. Branching ratios for the final: (a) $C(^1D)$, (b) $C(^3P)$, and (c) $C(^1P)$ states. Solid lines represent the results with capture in all doubly excited states. Dashed lines represent the results with capture only in the $2\ ^2\Pi$ dissociative state.

continuum, and partly validates our MQDT calculations of total DR, where the core-excited lowest Rydberg states were not included as dissociative channels.

(ii) The branching ratio does not change notably when the energy is varied around the resonance energies. The core excited bound Rydberg states $(a\ ^3\Pi)5s\sigma$ and $(A\ ^1\Pi)3p\sigma$ responsible for the structures in the total cross section (see Figs. 1 and 7) were explicitly included as closed channels in our close-coupling calculation, but the branching ratio does not change significantly across these resonances.

(iii) The large branching to the higher limit $C(^3D)$ found in the experiment results most probably from flux redistribution at long range ($R > 5$ a.u.). Indeed, the $^2\Pi$ valence state which correlates to this limit, not included in our calculations, does not enter the Franck-Condon region of the initial ion ground state ($v = 0$) at 1 eV. It can only receive flux from long range crossings (or avoided crossings) with lower Rydberg states.

These three remarks all converge to the same picture, at least for the CH^+ and CD^+ ions, of two rather distinct steps for the dissociative recombination process, based on two different regions of internuclear distance: the electron capture and autoionization is dominated by a few (one in the present case) specific dissociative channels at short distance, while

the flux redistribution towards various asymptotic limits results from multiple crossings at larger distance.

V. CONCLUSION

The main result of this paper is the assignment of the prominent structures observed at intermediate energies in the DR cross sections of CH^+ and CD^+ measured on the TSR storage ring [1,3]. As it was suggested in Ref. [3], they are due to electron capture into bound levels of core excited Rydberg states, which are then predissociated by the dominant dissociative state at low energy, the $2\ ^2\Pi$ state. The main feature of this core-excited indirect process for DR, compared to the resonant process involving nonadiabatic capture into monoexcited Rydberg states, is that here electronic interactions dominate both the recombination step and the predissociation step. The formation of these temporary doubly excited bound states does not seem to change notably the branching ratios for the dissociation to various atomic limits, which are dominated by long range multistate curve crossings. Some evidence has been found for non-adiabatic coupling leading to direct capture into mono-excited Rydberg states open for dissociation.

This core-excited indirect mechanism of dissociative recombination should occur for other molecular ions with low-lying bound excited states, as already observed in OH^+ DR [2]. It will not change the order of magnitude of the DR rates on a large energy domain, at least not at very low energy which is the most important for molecular abundances in interstellar clouds, but it can induce a substantial local increase of the cross section. The ''superexcited states'' responsible for this effect, subject to competing autoionization and predissociation (both via electronic couplings in the present case), should be important for photoionization and photodissociation studies in the adequate spectral range. Their observation in DR experiments can help or complete the identification of new structures in the ionization continuum of short-lived molecules, as studied recently by photoelectron spectroscopy using synchrotron radiation [28].

ACKNOWLEDGMENTS

We are very grateful to H. Takagi for communicating to us his data on CH potential curves, and to H. Lefebvre-Brion for many helpful discussions. We also thank Z. Amitay, U. Hechtfischer, and D. Zajfman for valuable informations about the experiments. A.S.-W. and I.F.S. thank I.N.S.U. for partial support. A.E.O. and L.C. acknowledge support from the National Science Foundation under Grant No. PHY-97-22136. Part of this work was performed under the auspices of the U.S. Department of Energy at Lawrence Livermore National Laboratory under Contract No. W-7450-Eng-48.

[1] P. Forck *et al.*, Phys. Rev. Lett. **72**, 2002 (1994).
[2] Z. Amitay *et al.*, Phys. Rev. A **53**, R644 (1996).
[3] Z. Amitay *et al.*, Phys. Rev. A **54**, 4032 (1996).
[4] L. Carata, I. F. Schneider, and A. Suzor-Weiner, Philos. Trans. R. Soc. London, Ser. A **355**, 1677 (1997).
[5] M. Larsson, Annu. Rev. Phys. Chem. **48**, 151 (1997).
[6] A. Suzor-Weiner and I. F. Schneider, in *Dissociative Recombination: Theory, Experiments and Applications III*, edited by D. Zajfman, J. B. A. Mitchell, D. Schwalm, and B. R. Rowe (World Scientific, Singapore, 1996), p. 1.
[7] A. Giusti-Suzor, J. Phys. B **13**, 3867 (1980); S. Guberman and A. Giusti-Suzor, J. Chem. Phys. **95**, 2602 (1991).
[8] S. L. Guberman, in *The Physics of Electronic and Atomic Collisions*, edited by L. J. Dubé, J. B. A. Mitchell, J. W. McConkey, and C. E. Brion, AIP Conf. Proc. No. 360 (AIP, New York, 1995), p. 314.
[9] T. Dunham, Publ. Astron. Soc. Pac. **49**, 26 (1937); P. Swings and L. Rosenfeld, Astrophys. J. **86**, 483 (1937).
[10] A. E. Douglas and G. Herzberg, Astrophys. J. **94**, 381 (1941).
[11] P. M. Mul, J. B. A. Mitchell, V. S. d'Angelo, P. Defrance, J. Wm. McGowan, and H. R. Froehlich, J. Phys. B **14**, 1353 (1981).
[12] J. N. Bardsley and B. R. Junker, Astrophys. J. Lett. **183**, L135 (1973).
[13] M. Krauss and P. S. Julienne, Astrophys. J. Lett. **183**, L139 (1973).
[14] A. Giusti-Suzor and H. Lefebvre-Brion, Astrophys. J. Lett. **214**, L101 (1977).
[15] H. Takagi, N. Kosugi, and M. Le Dourneuf, J. Phys. B **24**, 711 (1991).
[16] S. Green, P. S. Bagus, B. Liu, A. D. McLean, and M. Yoshimire, Phys. Rev. A **5**, 1614 (1972).
[17] B. Vâlcu, I. F. Schneider, M. Raoult, C. Strömholm, M. Larsson, and A. Suzor-Weiner, Eur. Phys. J. D **1**, 71 (1998).
[18] B. H. Lengsfield III, P. Saxe, R. Martin, and M. Page (unpublished).
[19] T. H. Dunning, J. Chem. Phys. **66**, 1382 (1977).
[20] G. Raseev, A. Giusti-Suzor, and H. Lefebvre-Brion, J. Phys. B **11**, 2735 (1978).
[21] V. Sidis and H. Lefebvre-Brion, J. Phys. B **4**, 1040 (1971).
[22] T. F. O'Malley, Phys. Rev. **150**, 14 (1966); **162**, 98 (1967).
[23] Ch. Jungen and O. Atabek, J. Chem. Phys. **66**, 5584 (1977); Ch. Jungen and D. Dill, **73**, 3338 (1980).
[24] E. F. van Dishoeck, J. Chem. Phys. **86**, 196 (1987).
[25] S. Cohen, Phys. Rev. A **13**, 99 (1976).
[26] D. Zajfman *et al.*, Phys. Rev. Lett. **79**, 1829 (1997).
[27] S. L. Guberman, Phys. Rev. A **49**, R4277 (1994).
[28] J. B. West, J. M. Dyke, A. Morris, T. G. Wright, and S. D. Gamblin, J. Phys. B **32**, 2763 (1999).